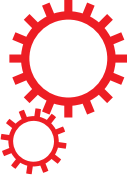


# SCIENTIFIC REPORTS



OPEN

## A Highly Responsive Silicon Nanowire/Amplifier MOSFET Hybrid Biosensor

Received: 13 December 2014

Accepted: 24 June 2015

Published: 21 July 2015

Jieun Lee<sup>1,2</sup>, Jaeman Jang<sup>1</sup>, Bongsik Choi<sup>1</sup>, Jinsu Yoon<sup>1</sup>, Jee-Yeon Kim<sup>3</sup>, Yang-Kyu Choi<sup>3</sup>, Dong Myong Kim<sup>1</sup>, Dae Hwan Kim<sup>1</sup> & Sung-Jin Choi<sup>1</sup>

This study demonstrates a hybrid biosensor comprised of a silicon nanowire (SiNW) integrated with an amplifier MOSFET to improve the current response of field-effect-transistor (FET)-based biosensors. The hybrid biosensor is fabricated using conventional CMOS technology, which has the potential advantage of high density and low noise performance. The biosensor shows a current response of 5.74 decades per pH for pH detection, which is  $2.5 \times 10^5$  times larger than that of a single SiNW sensor. In addition, we demonstrate charged polymer detection using the biosensor, with a high current change of  $4.5 \times 10^5$  with a 500 nM concentration of poly(allylamine hydrochloride). In addition, we demonstrate a wide dynamic range can be obtained by adjusting the liquid gate voltage. We expect that this biosensor will be advantageous and practical for biosensor applications which requires lower noise, high speed, and high density.

Highly sensitive biological detection is required for disease diagnosis<sup>1</sup>, drug discovery<sup>2</sup>, and biomolecular analysis<sup>3</sup>. The utilization of field-effect transistor (FET)-based sensor structures<sup>1,4-7</sup> has been one of the most promising solutions for label-free real-time detection compared with other biosensors, including surface plasmon resonance<sup>8</sup>, microcantilevers<sup>9</sup>, and an array of fluorescence sensors<sup>10</sup>. FET-based silicon nanowire (SiNW) biosensors have great potential due to advantages which include direct electrical read-outs, high sensitivity, and the potential to integrate them with complementary metal-oxide semiconductor (CMOS) circuits<sup>11-15</sup>.

SiNW biosensors operate by the change of current flowing through the SiNW channel which is induced by the change in surface charges, such as from a biomolecule binding reaction<sup>16</sup>. However, this current change often needs to be amplified, and in some applications current drive is important. Thus, the “current response”, which we define as the log of  $I/I_0$  per pH; (*i.e.* how many decades of current change per pH change), where  $I$  is the modified current and  $I_0$  is the initial current value, is an important metric. Many research groups have focused on efforts to improve current response. One of the most widely used methods is to reduce the doping concentration and nanowire width<sup>17,18</sup>. However, it is difficult to decrease the doping concentration of Si to below  $10^{15} \text{ cm}^{-3}$ . In addition, low fabrication yield and low reproducibility can be expected when decreasing the device width. Another way to increase current response is to control the operating bias point of the biosensor by tuning gate bias. The operation of the biosensor in the subthreshold region exhibits the highest current response (although with an increase in noise<sup>19</sup>), as has already been shown theoretically and experimentally<sup>20,21</sup>.

In the subthreshold region of FETs, the subthreshold swing (SS), *i.e.*, the inverse of the subthreshold slope, is defined as the gate voltage ( $V_G$ ) change needed to cause a one-order-of-magnitude change in the drain current and is expressed as

<sup>1</sup>School of Electrical Engineering, Kookmin University, Seoul 136-702, Republic of Korea. <sup>2</sup>Department of Electrical Engineering, Yale University, New Haven, Connecticut 06511, United States. <sup>3</sup>Department of Electrical Engineering, Korea Advanced Institute of Science and Technology, Daejeon 305-701, Korea. Correspondence and requests for materials should be addressed to S.-J.C. (email: sjchoie@kookmin.ac.kr)

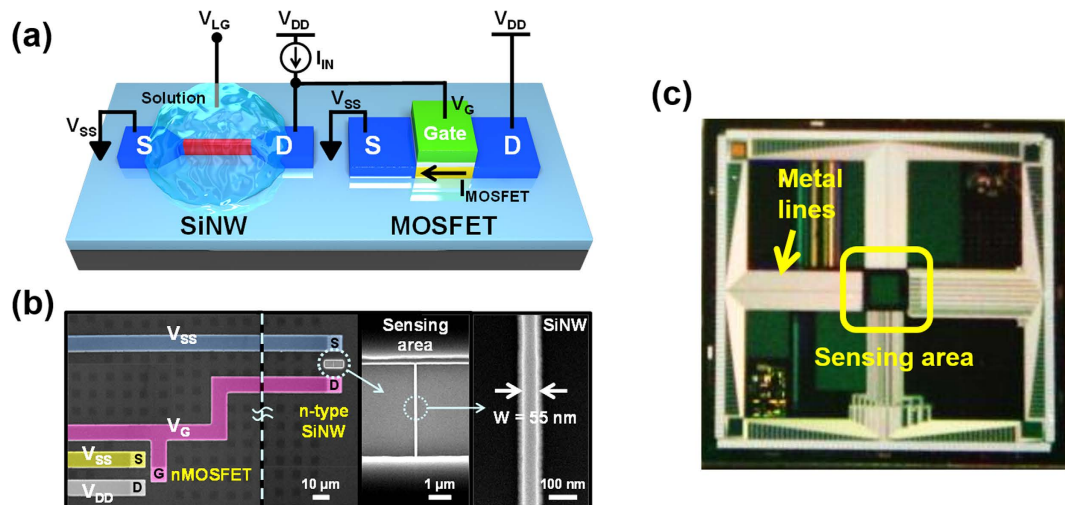


**Figure 1.** (a) Schematic diagram of the demonstrated biosensor composed of an n-type SiNW and a MOSFET. The SiNW is biased by  $V_{LG}$ , but the MOSFET is isolated from the solution. (b) False-colored scanning electron microscope images of the biosensor. The insets show a magnified view of the SiNW channel region ( $W = 55 \text{ nm}$ ). (c) Photograph of the biosensor chip fabricated via a top-down method.

$$SS = \frac{1}{Slope} = \frac{dV_G}{d(\log_{10}(I_D))} = 2.3m \frac{kT}{q}, \quad (1)$$

where  $k$  is the Boltzmann constant,  $T$  is the absolute temperature,  $q$  is the electric charge, and  $m$  is the ideality factor<sup>22</sup>. The minimum value of SS at room temperature can be achieved at 59.6 mV/decade when the minimum value of  $m$  is 1.

For pH sensors, which are the basis of broad sensor applications, the change in the surface potential of  $\text{SiO}_2$  with changing pH levels depends on the density and activation of surface sites, the buffer ionic strength, and the composition. The maximum change in the potential per pH is defined by the Nernst limit associated with an electrolyte and a site-binding surface, which is 59.6 mV/pH at room temperature<sup>23</sup>. Therefore, in the ideal case, the maximum ratio of current change ( $I/I_0$ ) per pH can intrinsically reach 10 (*i.e.*, 1 decade/pH) in the subthreshold region. However, because of sensor surface protonation affinity, the current change per pH with a  $\text{SiO}_2$  surface is always lower than the expected value<sup>23</sup>. In this paper, we demonstrate a new type of hybrid biosensor that combines the SiNW and conventional MOSFET, serving as an amplifier, to exceed the aforementioned current response intrinsic limit of 1 decade/pH. We demonstrate that the current response of the hybrid biosensor can be amplified considerably beyond the current response limit of the single SiNW biosensor. In addition, the hybrid biosensor is monolithically integrated on the same wafer using conventional top-down CMOS technology, indicating that it will be able to have the lower noise performance of amplification compared with laboratory instruments.

A schematic of the hybrid SiNW-MOSFET biosensor is shown in Fig. 1a. In this configuration, the SiNW device plays the role of a sensor and is exposed to the solution, whereas the MOSFET acts as a transducer to amplify the current response and is insulated from the solution. The SiNW and MOSFET are monolithically integrated and electrically connected by a metal line using conventional CMOS technology. The gate of the MOSFET and the drain of the SiNW FET are connected and are driven by the current source ( $I_{IN}$ ). Therefore, the drain voltage of the SiNW FET can be varied according to the conductance of the SiNW, which can control the gate voltage ( $V_G$ ) of the MOSFET. Figure 1b shows scanning electron microscope (SEM) images of the fabricated hybrid SiNW-MOSFET biosensor. The passivation layer around the SiNW channel region was removed to enable sensing, whereas regions outside the SiNW channel are passivated with a  $\text{SiO}_2$  layer to prevent leakage current through solution. The sensing area is located at the center of the chip, and all metal lines are extended to the edge of the chip to isolate the probe tips from the solution (Fig. 1c). Details of the fabrication process are discussed in Supplementary Figure S1 online.

## Results and Discussion

We first used the pH-sensing experiment as a model system to study the response of our hybrid SiNW and MOSFET biosensor. In these experiments, the  $\text{SiO}_2$  surface of the SiNWs were modified with 3-aminopropyltriethoxysilane (APTES). The SiNW surface was exposed to 0.1X potassium phosphate buffer solutions with five different pH values (*i.e.*, pH 5, 6, 7, 8, and 9) by a microfluidic channel (see

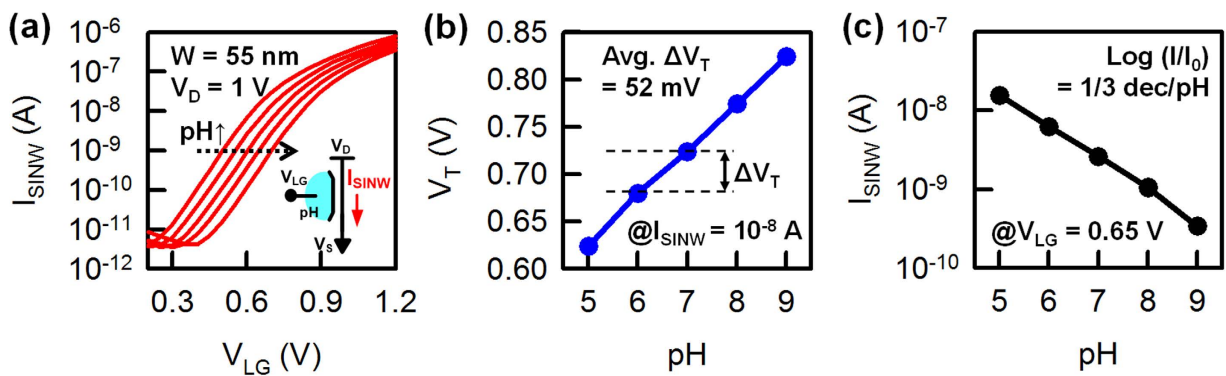


**Figure 2.** (a) Transfer characteristics of an n-type single SiNW FET as a pH sensor with a sweeping  $V_{\text{LG}}$ . The SiNW FET was functionalized with APTES to apply amine ( $-\text{NH}_2$ ) groups to the sensor surface. The SS of the SiNW FET is  $147 \text{ mV/decade}$ . (b)  $V_T$  and (c)  $I_{\text{SiNW}}$  at different pH levels; these values were extracted from Fig. 2a.  $V_T$  was extracted using the constant current method at  $I_{\text{SiNW}} = 10^{-8} \text{ A}$ , and the current response ( $\log(I/I_0)$ ) was extracted from the transfer characteristics at  $V_{\text{LG}} = 0.65 \text{ V}$ .

Supplementary Figure S2 online). In the pH experiment of a single SiNW FET with an electrolyte gate (*i.e.*, a liquid gate), we used an n-type SiNW. The drain current flowing through the SiNW channel ( $I_{\text{SiNW}}$ ) was measured at a constant drain voltage ( $V_D$ ) of 1 V while the liquid gate voltage ( $V_{\text{LG}}$ ) was swept from 0 to 1.2 V with 25 mV steps. The transfer characteristics of the n-type SiNW FET for the five different pH values are shown in Fig. 2a. The gate leakage current in this work is negligible (see Supplementary Figure S3 online). The pH responses are stable and repeatable over many hours of operations. As the pH level increases, the conductance of the n-type SiNW FET decreases, resulting in a positive shift of the threshold voltage ( $V_T$ ). This can be explained by the protonation/deprotonation of  $-\text{NH}_2$  and  $-\text{SiOH}$  groups on the functionalized SiNW surface. At low pH levels, the  $-\text{NH}_2$  group is protonated to  $-\text{NH}_3^+$ , resulting in a positive charge. In contrast, at high pH levels, the  $-\text{SiOH}$  group is deprotonated to  $-\text{SiO}^-$  and results in a negative charge<sup>23</sup>. The average  $V_T$  shift is 52 mV per pH (Fig. 2b), which is below the Nernst limit as expected. In addition, the SS of the single SiNW FET with the liquid gate is  $147 \text{ mV/decade}$ , which is considerably larger than that of the ideal value ( $59.6 \text{ mV/decade}$ ). In the subthreshold region, the extracted current response (how many decades per pH) of the single SiNW FET is approximately  $1/3$  decade per pH (Fig. 2c), which is smaller than the ideal current response of 1 decade per pH. Therefore, it is difficult for the single SiNW FET to achieve a higher current response because of the smaller  $V_T$  shift and the larger SS than the expected values, which is caused by non-ideal interfaces between the gate insulator layer and the electrolyte<sup>23</sup>.

Figure 3 presents the experimental results for the SiNW/MOSFET hybrid pair biosensor, demonstrating a high current response for pH changes. To understand the overall response of the biosensor, we first characterize the voltage transfer curves,  $V_{\text{LG}}$  versus  $V_G$ , for different pH levels, as shown in Fig. 3a. In the measurement, the current source ( $I_{\text{IN}}$ ) is set to 1 nA, and the  $V_G$  node is limited to 1 V using the voltage compliance of the measurement equipment (4156C, Agilent). At low  $V_{\text{LG}}$  (*i.e.*, the off-state of the SiNW FET), it is difficult to discharge the forced current  $I_{\text{IN}}$  into the ground through the SiNW channel because the conductance of the SiNW remains low. Thus, the  $V_G$  node maintains a 'HIGH' ( $= 1 \text{ V}$ ) level. However,  $V_G$  rapidly changes from 'HIGH' to 'LOW' ( $= 0 \text{ V}$ ) at a specific  $V_{\text{LG}}$  point because the conductance of the SiNW becomes sufficiently large (*i.e.*, the on-state of the SiNW FET) to discharge  $I_{\text{IN}}$ . Therefore, the rapid change of  $V_G$  is expected to be able to effectively change the output current ( $I_{\text{MOSFET}}$ ) in the MOSFET at the specific  $V_{\text{LG}}$  point.

Figure 3b shows the resulting output current ( $I_{\text{MOSFET}}$ ) of the MOSFET in our hybrid sensor. At low  $V_{\text{LG}}$ ,  $I_{\text{MOSFET}}$  remains high ( $5.5 \times 10^{-7} \text{ A}$ ) because of the high  $V_G$  value at this point. However,  $I_{\text{MOSFET}}$  abruptly drops to a low level ( $10^{-12} \text{ A}$ ) at a specific  $V_{\text{LG}}$ , as expected. As a result, we achieve a large current change ( $I/I_0$ ) with varying pH levels (approximately  $5.5 \times 10^5 \text{ pH}$ ) at a fixed  $V_{\text{LG}}$  value (note the vertical arrow between pH curves in Fig. 3b). As shown in Fig. 3b, the current change of the hybrid biosensor is saturated, since this  $I/I_0$  is strongly affected by the on/off current ratio of the MOSFET (see Supplementary Figure S4 online); therefore,  $I/I_0$  can be further increased by improving the performance of the MOSFET.

Figure 3c shows  $I_{\text{MOSFET}}$  versus time with varying pH levels at the fixed  $V_{\text{LG}}$  value. Noise spikes occur every 100 s when the pH values are changed; however, the  $I_{\text{MOSFET}}$  quickly equilibrates. A clear amplified signal is obtained for the different pH levels by adjusting  $V_{\text{LG}}$ , *i.e.*,  $I/I_0 \sim 5.5 \times 10^5$ , as shown in Fig. 3c. The hybrid biosensor gives a current response of 5.74 decade per pH, as compared to the small pH response of a single SiNW FET (a current response of  $1/3$  decade per pH). Finally, the extracted current response of the hybrid pH sensor and the conventional SiNW pH sensor alone are compared in Fig. 3d. The red symbols show the current response measured for the single SiNW FET as a function of

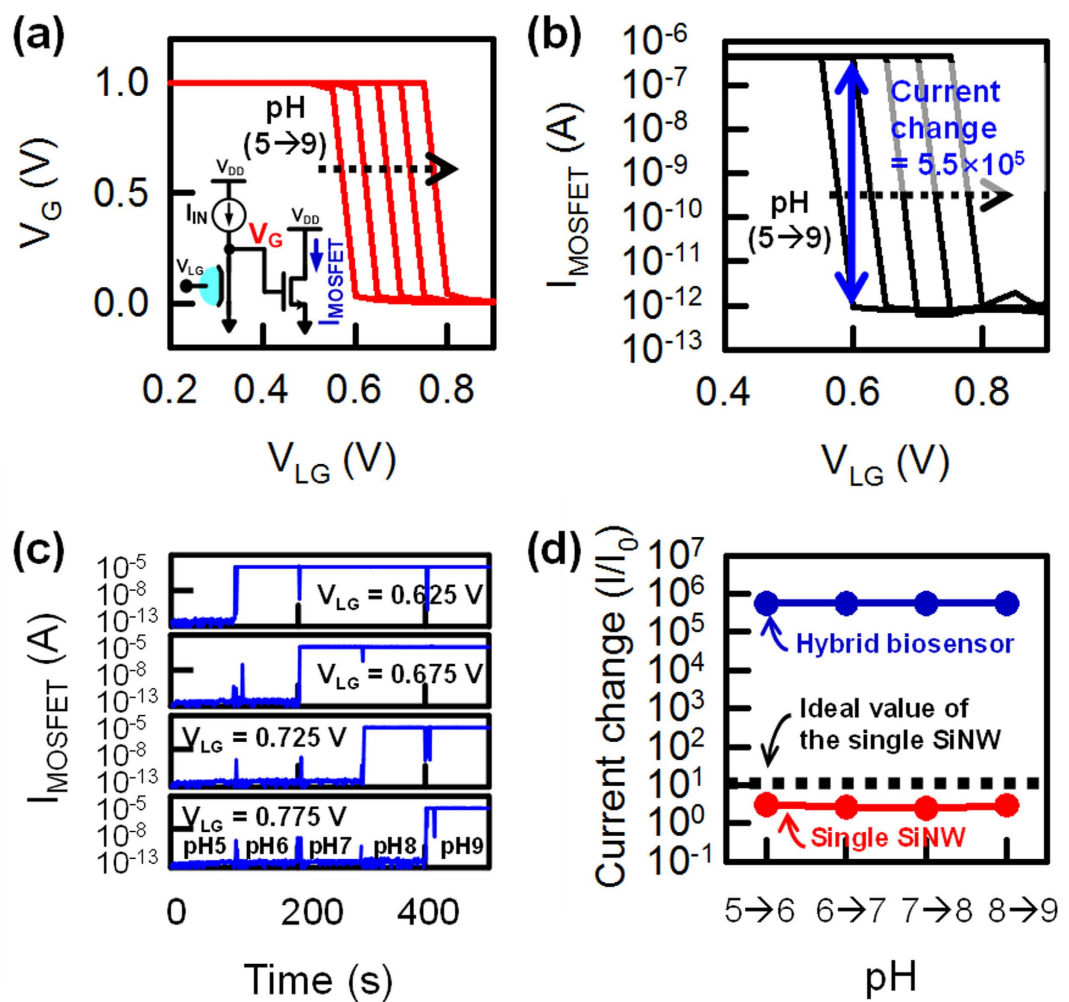


**Figure 3. Measured electrical characteristics of the hybrid silicon nanowire (SiNW)-MOSFET biosensor as a pH sensor.** (a)  $V_G$  of the hybrid biosensor while varying the pH from 5 to 9. (b) MOSFET output current ( $I_{MOSFET}$ ) as a function of pH level in the hybrid biosensor. The extracted current change is  $5.5 \times 10^5$  ( $= 5.74$  decade per pH). (c) Transient response of  $I_{MOSFET}$  while varying the pH in the hybrid biosensor. (d) Measured current change depending on the biosensor types, *i.e.*, the single SiNW biosensor and the hybrid biosensor. The dashed black line indicates the maximum current response according to the Nernst limit.

pH. The current response is extracted from the transfer curves of the single SiNW biosensor in Fig. 2a at  $V_{LG} = 0.65$  V. The dashed black line represents the aforementioned ideal current response of a single SiNW FET. The current response of the hybrid biosensor is represented by blue dots, demonstrating a current response approximately  $2.5 \times 10^5$  times greater than that of the single SiNW pH sensor. It is important to note that the hybrid biosensor has the wide dynamic range by shifting the liquid gate voltage (Fig. 3a). Importantly, we expect that a small threshold voltage shift (a change of 20 mV), corresponding to a 0.34 pH change, can be detected with the high current response of the hybrid biosensor, as shown in Supplementary Figure S5 online. This simulation also shows that we expect a smaller threshold voltage shift (less than  $\Delta pH < 0.34$ ) should be detectable (Supplementary Figures S6 and S7 online). Thus, the hybrid biosensor can simply produce a dramatic amplification of the current response without additional off-chip circuitry.

To further evaluate the advantages of our hybrid sensor, we detected charged molecules, specifically poly(sodium styrene sulfonate) (PSS) and poly(allylamine hydrochloride) (PAH), which are oppositely charged. The PSS polymer is negatively charged, whereas the PAH polymer is positively charged, and layer-by-layer build-up is a straightforward protocol<sup>24–26</sup>. To detect the positive charges of the PAH polymer, the PSS polymers were pre-applied to the positively charged APTES-modified  $\text{SiO}_2$  surface. Next, the PAH polymer was attached on the PSS layer. The experimental procedure is explained in detail in Supplementary Figure S8 online. Figure 4 demonstrates the experimental validation of charged polymer detection using the single SiNW biosensor. The transfer curves of the n-type single SiNW FET with varying PAH concentrations are shown in Fig. 4a. The attachment of the positively charged PAH results in a negative  $V_T$  shift because the attached positively charged PAH can accumulate more electron

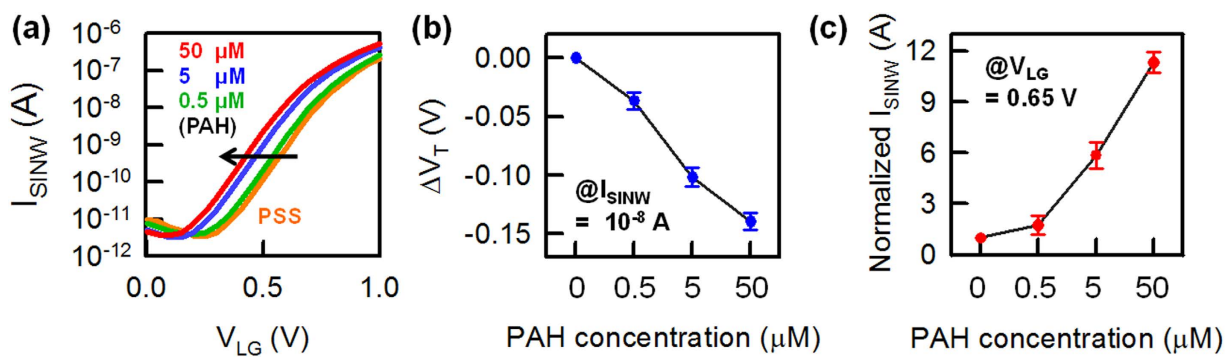


**Figure 4. Measured electrical characteristics of the single SiNW FET as a function of PAH concentration.** (a) Transfer curves of the single SiNW biosensor with increasing PAH concentration. (b)  $V_T$  shift and (c) normalized  $I_{SiNW}$  are extracted from the transfer curves of the SiNW biosensors. The measured data from six devices are included in each condition.

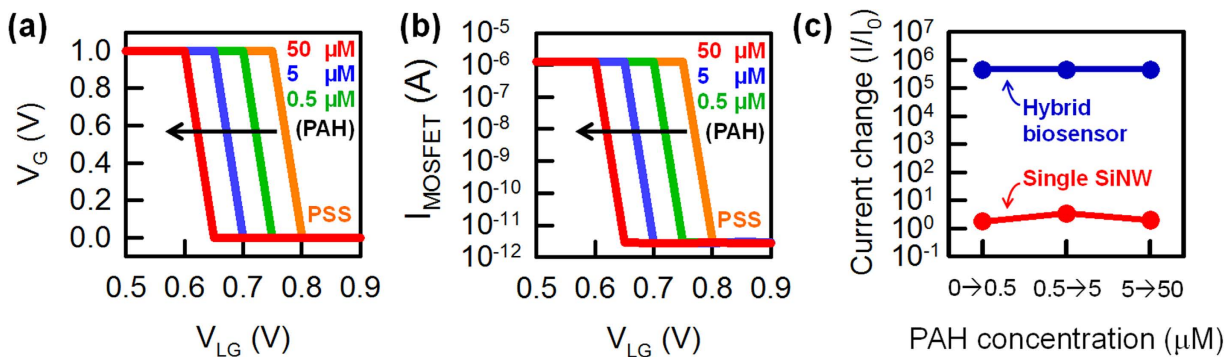


**Figure 5. Measured electrical characteristics of the hybrid biosensor as a function of PAH concentration.** (a)  $V_G$ - $V_{LG}$  and (b)  $I_{MOSFET}$ - $V_{LG}$  characteristics of the hybrid biosensor with varying PAH concentrations. (c) Comparison of the current change for the two biosensor types at different PAH concentrations.

carriers in the n-type SiNW channel. Thus, as the PAH concentration increases, the  $V_T$  of the n-type SiNW biosensor is more negatively shifted and the current flowing to the SiNW (*i.e.*,  $I_{SiNW}$ ) increases correspondingly (Fig. 4b,c). In this case, the average  $\Delta V_T$  is 38 mV at the lowest PAH concentration (500 nM), and the measured average current change is 2.7. Figure 5a shows that the  $V_G$ - $V_{LG}$  curves of the hybrid biosensor are negatively shifted with changing PAH concentration. The  $I_{MOSFET}$ - $V_{LG}$  curve is also shifted depending on the  $V_G$ - $V_{LG}$  curve shift. Therefore, similar to the pH experiment, the hybrid biosensor can obtain a large amplification in current change ( $= 4.5 \times 10^5$  at a PAH of 500 nM) compared with a single SiNW FET at a fixed  $V_{LG}$ , as shown in Fig. 5b. The current change for two types of biosensors (*i.e.*, a single SiNW and the hybrid sensor) at different PAH concentrations are summarized in Fig. 5c. The red symbols show the current response measured in the single SiNW biosensor with varying PAH concentrations at  $V_{LG} = 0.65$  V. The blue symbols represent the current response of the hybrid biosensor. The experimental results demonstrate that the hybrid biosensor can dramatically increase the current response for charged polymer detection. The high current response of the hybrid biosensor as demonstrated here should be applicable to other biomolecule detection systems.

## Conclusions

In this paper, we demonstrated a hybrid biosensor composed of a single SiNW and a single amplifier MOSFET. We show that the hybrid biosensor offers remarkable amplification of the current response in both pH and charged polymer detection, which is more than  $2.5 \times 10^5$  times larger than a single SiNW sensor counterpart. Furthermore, the demonstrated biosensor shows a wide detection dynamic range by adjusting the liquid gate voltage. We believe that this is the first report of a high responsivity, large dynamic range amplifier monolithically integrated with a biosensor, which should be advantageous and practical for biosensor applications which requires lower noise, high speed, and high density. Given its compatibility with conventional top-down CMOS processing technology, this biosensor should have wide applicability for biomedical and chemical sensors.

## References

1. Zheng, G., Patolsky, F., Cui, Y., Wang, W. U. & Lieber, C. M. Multiplexed Electrical Detection of Cancer Markers with Nanowire Sensor Arrays. *Nat. Biotechnol.* **23**, 1294–1301 (2005).
2. Wang, W. U., Chen, C., Lin, K.-h., Fang, Y. & Lieber, C. M. Label-free detection of small-molecule-protein interactions by using nanowire nanosensors. *Proc. Natl. Acad. Sci. USA* **102**, 3208–3212 (2005).
3. Bergveld, P. Development, Operation, and Application of the Ion-Sensitive Field-Effect Transistor as a Tool for Electrophysiology. *IEEE Trans. Biomed. Eng.* **19**, 342–351 (1972).
4. Stern, E. *et al.* Label-free immunodetection with CMOS-compatible semiconducting nanowires. *Nature* **445**, 519–522 (2007).
5. Patolsky, F. & Lieber, C. M. Nanowire nanosensors. *Mater. Today* **8**, 20–28 (2005).
6. Ramachandran, N., Larson, D. N., Stark, P. R. H., Hainsworth, E. & LaBaer, J. Emerging tools for real-time label-free detection of interactions on functional protein microarrays. *FEBS J.* **272**, 5412–5425 (2005).
7. Cheng, Y. *et al.* Mechanism and Optimization of pH Sensing Using  $\text{SnO}_2$  Nanobelt Field Effect Transistors. *Nano Lett.* **8**, 4179–4184 (2008).
8. Scanrano, S., Mascini, M., Turner, A. P. F. & Minunni, M. Surface plasmon resonance imaging for affinity-based biosensors. *Biosens. Bioelect.* **25**, 957–966 (2010).
9. Buchapudi, K. R., Huang, X., Yang, X., Ji, H.-F. & Thundat, T. Microcantilever biosensors for chemicals and bioorganisms. *Analyst* **136**, 1539–1556 (2011).
10. Bruno, A. E. *et al.* All-Solid-State Miniaturized Fluorescence Sensor Array for the Determination of Critical Gases and Electrolytes in Blood. *Anal. Chem.* **69**, 507–513 (1997).
11. Cui, Y., Wei, Q., Park, H. & Lieber, C. M. Nanowire Nanosensors for Highly Sensitive and Selective Detection of Biological and Chemical Species. *Science* **293**, 1289–1292 (2001).
12. Ahn, J.-H. *et al.* Double-Gate Nanowire Field Effect Transistor for a biosensor. *Nano Lett.* **10**, 2934–2938 (2010).
13. Gao, A. *et al.* Enhanced Sensing of Nucleic Acids with Silicon Nanowire Field Effect Transistor Biosensors. *Nano Lett.* **12**, 5262–5268 (2012).
14. Lee, J. *et al.* A Novel SiNW/CMOS Hybrid Biosensor for High Sensitivity/Low Noise. *59th IEEE International Electron Device Meeting (IEDM)*, Washington DC, USA, 385–388 (2013).
15. Park, I., Li, Z., Pisano, A. P. & Williams, R. S. Top-down fabricated silicon nanowire sensors for real-time chemical detection. *Nanotechnol.* **21**, 015501-1–015501-9 (2010).
16. Curreli, M., Thompson, M. E. *et al.* Real-Time, Label-Free Detection of Biological Entities Using Nanowire-Based FETs. *IEEE Trans. Nanotechnol.* **7**, 651–667 (2008).
17. Elfström, N. *et al.* Surface Charge Sensitivity of Silicon Nanowires: Size Dependence. *Nano Lett.* **7**, 2608–2612 (2007).
18. Nair, P. R. & Alam, M. A. Design Considerations of Silicon Nanowire Biosensors. *IEEE Trans. Elect. Dev.* **54**, 3400–3408 (2007).
19. Rajan, N. K., Routenberg, D. A. & Reed, M. A. Optimal signal-to-noise ratio for silicon nanowire biochemical sensors. *Appl. Phys. Lett.* **98**, 264107 (2011).
20. Gao, X. P. A., Zheng, G. & Lieber, C. M. Subthreshold Regime has the Optimal Sensitivity for Nanowire FET Biosensors. *Nano Lett.* **10**, 547–552 (2010).
21. Lu, M.-P., Hsiao, C.-Y., Lai, W.-T. & Yang, Y.-S. Probing the sensitivity of nanowire-based biosensors using liquid-gating. *Nanotechnol.* **21**, 425505-1–205505-425505-5 (2010).
22. Taur, Y. & Ning, T. H. *Fundamentals of Modern VLSI Devices*, Cambridge University Press, Cambridge, 1998.
23. Bousse, L., Rooij, N. F. D. & Bergveld, P. Operation of chemically sensitive field-effect sensors as a function of the insulator-electrolyte interface. *IEEE Trans. Elect. Dev. ED-30*, 1263–1270 (1983).
24. Riegler, H. & ESSLER, F. Polyelectrolytes. 2. Intrinsic or Extrinsic Charge Compensation? Quantitative Charge Analysis of PAH/PSS Multilayers. *Langmuir* **18**, 6694–6698 (2002).
25. Uslu, F. *et al.* Label-free fully electronic nucleic acid detection system based on a field-effect transistor device. *Biosens. Bioelect.* **19**, 1723–1731 (2004).
26. Vu, X. T., Stockmann, R., Wolfrum, B., Offenhäusser, A. & Ingebrandt, S. Fabrication and application of a microfluidic-embedded silicon nanowire biosensor chip. *Phys. Status Solidi A* **207**, 850–857 (2010).

## Acknowledgements

This work was supported in part by the National Research Foundation of Korea through the Ministry of Education, Science and Technology, Korean Government, under Grant 2014064116 and Grant 2013065339, in part by the Center for Integrated Smart Sensors funded by the Ministry of Science, ICT & Future Planning as Global Frontier Project (CISS-2011-0031848), and in part by U.S. Army Research Office and Air Force Research Laboratory, under contract/grant number MURI W911NF-11-1-0024. We would like to thank Professor Mark A. Reed for useful discussions.

## Author Contributions

J.L. and S.-J.C. conceived the idea and wrote the main manuscript text. J.L. and J.J. conducted the electrical measurement and SPICE simulation. B.C., J.Y. and J.-Y.K. contributed to experimental design. Y.-K.C., D.M.K. and D.H.K. contributed for the editing of the manuscript. All authors discussed the results and reviewed the manuscript.

## Additional Information

**Supplementary information** accompanies this paper at <http://www.nature.com/srep>

**Competing financial interests:** The authors declare no competing financial interests.

**How to cite this article:** Lee, J. *et al.* A Highly Responsive Silicon Nanowire/Amplifier MOSFET Hybrid Biosensor. *Sci. Rep.* **5**, 12286; doi: 10.1038/srep12286 (2015).



This work is licensed under a Creative Commons Attribution 4.0 International License. The images or other third party material in this article are included in the article's Creative Commons license, unless indicated otherwise in the credit line; if the material is not included under the Creative Commons license, users will need to obtain permission from the license holder to reproduce the material. To view a copy of this license, visit <http://creativecommons.org/licenses/by/4.0/>